

## THE USEFULNESS OF A 400 kV HIGH-RESOLUTION ANALYTICAL ELECTRON MICROSCOPE

Y. BANDO, Y. MATSUI and Y. UEMURA

*National Institute for Research in Inorganic Materials, 1-Namiki, Sakura-mura, Niihari-gun, Ibaraki 305, Japan*

and

T. OIKAWA, S. SUZUKI, T. HONDA and Y. HARADA

*JEOL Ltd., 1418 Nakagami, Akishima, Tokyo 196, Japan*

Received 3 June 1985; presented at Symposium January 1985

In order to show the usefulness of a 400 kV high-resolution analytical electron microscope (JEM-4000EX), the accelerating voltage dependence of the peak-to-background ratio in both energy-dispersive X-ray spectroscopy (EDXS) and electron energy-loss spectroscopy (EELS) is studied. It is shown that the peak-to-background ratios increase continuously with increase of the accelerating voltage from 100 to 400 kV. It is also shown that both crystal structure and chemical composition of 15R sialon polytype ( $\text{SiAl}_4\text{O}_2\text{N}_4$ ) may be determined on the basis of structure images and quantitative analysis of the corresponding EDXS and EELS spectra, demonstrating the capability of the combined techniques of high-resolution imaging and microanalysis.

### 1. Introduction

In recent years, electron microscopes have come into widespread use as microanalytical tools. An energy-dispersive X-ray spectrometer (EDXS) and an electron energy-loss spectrometer (EELS) can be applied to carry out qualitative or quantitative analysis from small regions in thin specimens. However, the conventional TEM-STEM analytical electron microscope has three disadvantages at 100 or 200 kV. (1) The image resolution in TEM is not high as compared to normal transmission electron microscopes. Thus the combined use of structure imaging and microanalysis is not applicable. (2) The peak-to-background ratio ( $P/B$ ) is not high in the EDXS and the EELS spectra, which restricts the detection sensitivity for any elements present in small quantities. Especially in the EELS spectra, characteristic energy-loss peaks are always placed on a high background. The latter is related to multiple inelastic scattering electrons, mainly due to volume plasmons. (3) The spatial resolution

for microanalysis degrades due to electron beam spreading in thin specimens.

As has been already pointed out [1,2], the designed observation capabilities can be very much improved by increasing the accelerating voltage. From this point of view, a newly constructed TEM-STEM analytical electron microscope, with a medium voltage of 400 kV (JEM-400EX) [3], should be more useful. In previous papers [4,5], some instrumental features of the JEM-400EX have been described. It has been demonstrated that the 400 kV analytical electron microscope is fully capable of observing crystal structure images of inorganic compounds.

In the present paper, we demonstrate some of the advantages of the 400 kV high-resolution analytical electron microscope. It is shown that the  $P/B$  ratios for both EDXS and EELS increase with accelerating voltages from 100 to 400 kV. The present microscope also enables us to combine structure imaging and microanalysis without changing objective polepieces. Thus the crystal

structure and chemical composition of 15R sialon polytype ( $\text{SiAl}_4\text{O}_2\text{N}_4$ ) could be determined.

## 2. Instrumental features of the 400 kV analytical electron microscope

### 2.1. Microscope

Details of the 400 kV high-resolution analytical electron microscope (JEM-4000EX) have been described by Hashimoto et al. [3] and the present authors [5]. Here, we describe briefly some features of the JEM-4000EX analytical systems. The side-entry specimen holder has a specimen retainer made of beryllium which can be tilted by  $30^\circ$  for both  $X$  and  $Y$ . The spherical and chromatic aberration coefficients are presently 3.3 and 2.6 mm, respectively. The beam convergence half-angle and the energy spread of the  $\text{LaB}_6$  gun source are estimated to be 1.0 mrad and 1.5 eV, respectively. According to calculations of the phase contrast transfer function, including the envelope function due to partial coherence and chromatic aberration effect, the theoretical resolution limit is estimated to be 0.23 nm at the optimum Scherzer defocus of about 90 nm [4].

The EDXS (Tracor Northern X-ray) is placed at a high take-off angle position of  $65^\circ$  with a collection angle of 0.029 str. The EELS spectrometer (ASEA40) is attached to the microscope column, which is also interfaced with a scanning image device (ASID40). The energy resolutions obtained are 1.6 and 1.8 eV at 200 and 400 kV, respectively [5]. The spectra are acquired into 1024 channels of a TN2000 minicomputer-based multi-channel scaler in order to carry out qualitative or quantitative analysis of the spectra. A Faraday cup is set in side-entry specimen holder to measure the electron probe current adjusted to the specimen. The vacuum at the gun chamber and near the specimen are currently  $1.4 \times 10^{-7}$  and  $4.0 \times 10^{-7}$  Torr, respectively.

At higher voltages, stray radiation originating from the high-energy electron beams may cause systematic errors. To overcome these problems, two modifications to the microscope column were made. One is to reduce Bremsstrahlung production

and the other is to protect the EDXS detector from hard X-ray radiation coming from the upper parts of the column, mainly from the condenser lens aperture. In order to reduce Bremsstrahlung, many parts of the column wall which electron beams might hit were covered with graphite, and the light elements were used for the condenser aperture. To protect the detector, X-ray shielding made of heavy metals such as W, Ta and Pb, with total thickness of more than 30 mm, were set between the condenser aperture and the detector.

### 2.2. The increase of the peak-to-background ratio with accelerating voltages

Fig. 1a shows the EDXS spectra from a 50 nm thick vapour-deposited Ge film mounted on a beryllium microscope grid, observed at various accelerating voltages between 100 and 400 kV. The probe current and the probe diameter are approximately 20 nA and 2  $\mu\text{m}$ , respectively, and were maintained constant at each operating voltage. As can be seen in fig. 1a, the intensities of the characteristic  $\text{Ge}_L$  and  $\text{Ge}_K$  lines decrease with increasing voltages, whereas those of L lines decrease more rapidly than those of K lines. In order to see the effect of stray X-rays, the spectra are shown enlarged with the vertical full scale in fig. 1b. The weak characteristic peaks located at 1.74 and 3.74 keV are corresponding to  $\text{Si}_K$  and  $\text{Ag}_L$  lines, which are generated from impurities of the specimen. Cu peaks are identified as spurious instrumental X-ray peaks. These are always observed in the spectra for 100 to 400 kV. These may be caused by irradiation of the specimen holder. No other spurious X-ray peaks were observed, suggesting that stray radiation shielding has been achieved successfully at 400 kV.

Fig. 2 shows the accelerating voltage dependence of the characteristic X-ray counts, the background counts (BGD), and the total counts, obtained from fig. 1. The characteristic peak intensities for  $\text{Ge}_L$  and  $\text{Ge}_K$  lines are integrated over energy ranges between 0.94 and 1.34 keV, and between 9.68 and 10.08 keV, respectively, with energy width of 400 eV. The background intensity was measured in the range between 7.00 and 7.40 keV. The total counts were integrated from 0 to 20

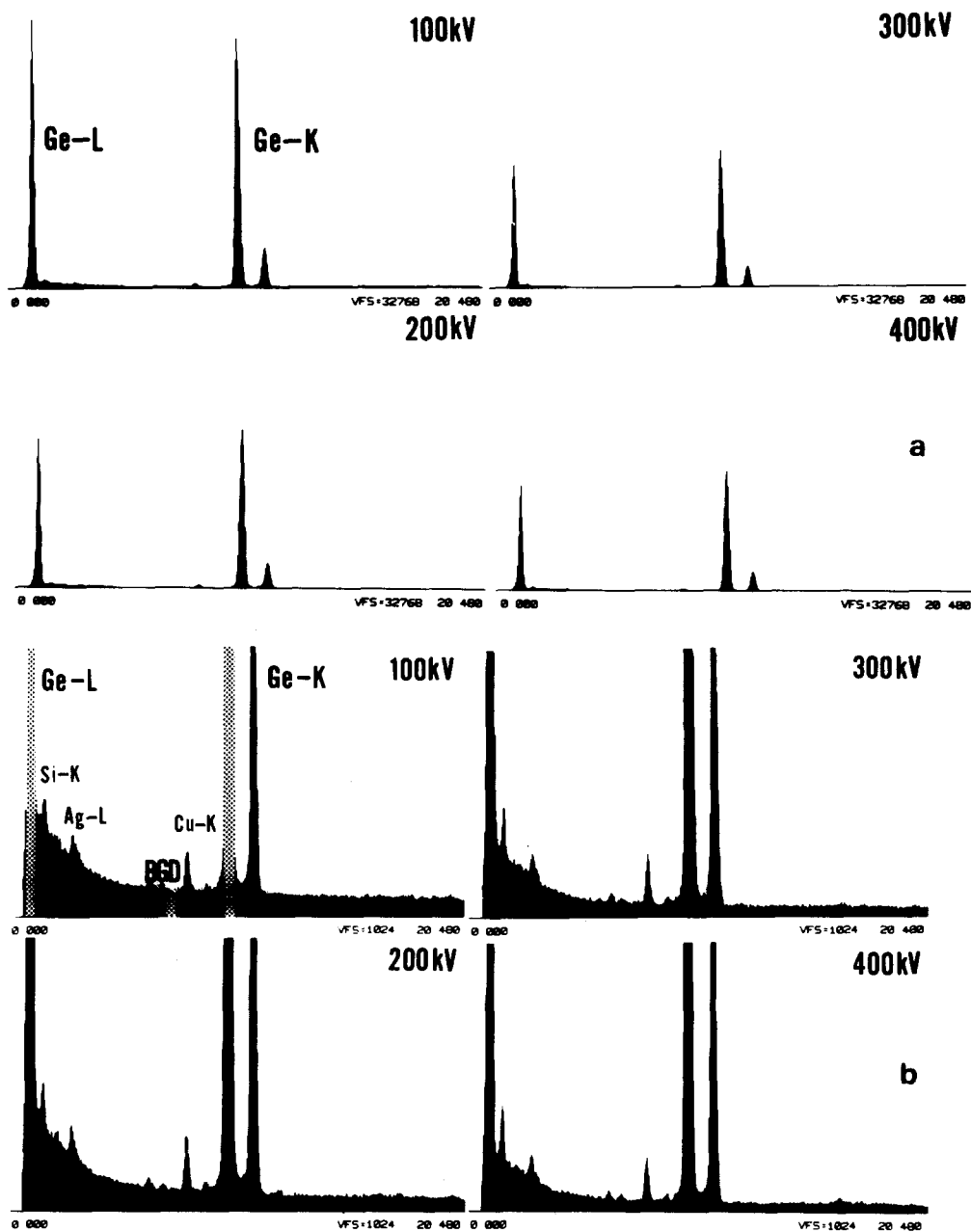


Fig. 1. EDXS spectra from a vapour-deposited 50 nm thick Ge film, observed at various accelerating voltages between 100 and 400 kV (a). The same spectra are enlarged with the vertical full scale in (b). The probe current and the probe diameter of 20 nA and 2  $\mu$ m, respectively, were kept the same at each voltage.

keV, including the characteristic X-rays and the background. It can be seen that the characteristic intensities decrease very rapidly between 100 and 200 kV, but not so rapidly above 200 kV. On the

other hand, the background also decreases with increase of the accelerating voltage and it decreases more rapidly than the characteristic X-rays. As a result, the peak-to-background ratio ( $P/B$ )

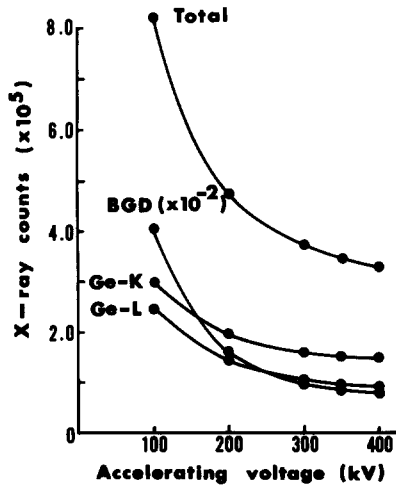


Fig. 2. The accelerating voltage dependence of X-ray production for  $\text{Ge}_K$ ,  $\text{Ge}_L$  and of the total and the background (BGD), deduced from fig. 1.

increases continuously with increase of the accelerating voltage as shown in fig. 3. The  $P/B$  ratios observed at voltages of 100, 200, 300 and 400 kV are 75, 122, 156 and 177 for the  $\text{Ge}_K$  line and 63, 89, 109 and 119 for the  $\text{Ge}_L$  line, respectively. The  $P/B$  ratio at 400 kV is then approximately 2 times higher than at 100 kV.

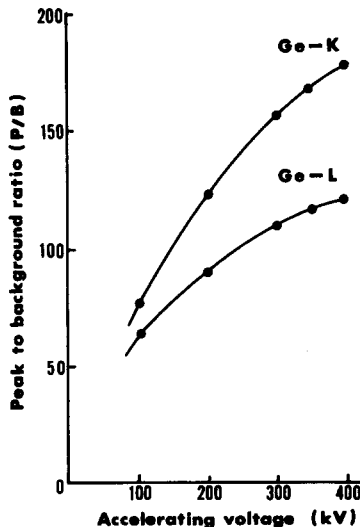


Fig. 3. The peak-to-background ratio ( $P/B$ ) observed for the  $\text{Ge}_K$  and the  $\text{Ge}_L$  lines as a function of the accelerating voltages.

Fig. 4 shows EELS spectra consisting of zero-loss and plasmon-loss peaks from a 200 nm thick evaporated Al film, obtained at various accelerating voltages. The spectra are observed with a cut-off angle of about 4.8 mrad. The intensity ratio of the plasmon-loss peak to the zero-loss peak decreases with the accelerating voltages.

Fig. 5 shows a comparison between calculated and experimental mean-free-path lengths of Al plasmon excitations as a function of the cut-off angle with various accelerating voltages. The mean free path of the volume plasmon ( $\lambda_p$ ) can be calculated [6] using

$$\lambda_p = \frac{a_0}{\theta_e \ln(\theta_c + \theta_e)}, \quad (1)$$

$$\theta_e = \frac{hw_p(1 + 2\epsilon E_0)}{2E_0(1 + \epsilon E_0)}, \quad (2)$$

where  $a_0$  is the Bohr radius,  $\theta_e$  is the characteristic scattering angle,  $\theta_c$  is the cut-off angle,  $hw_p$  is the

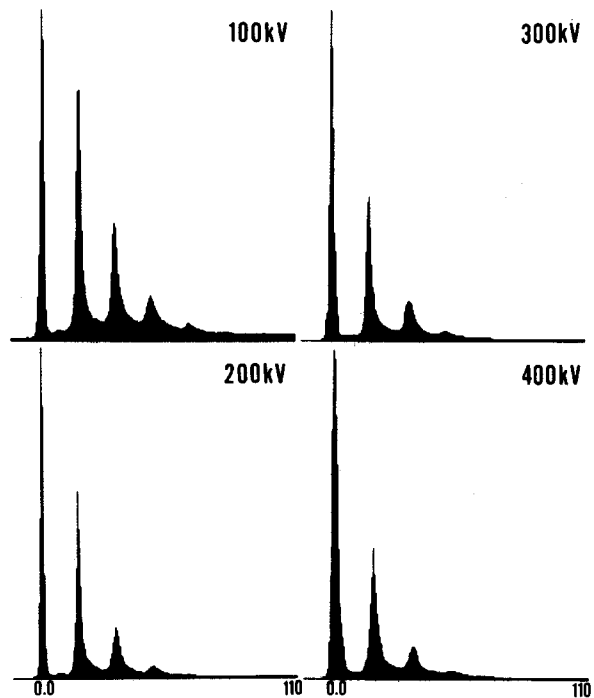


Fig. 4. EELS spectra from a 200 nm thick evaporated Al film, consisting of zero-loss and plasmon-loss peaks, observed at voltages from 100 to 400 kV.

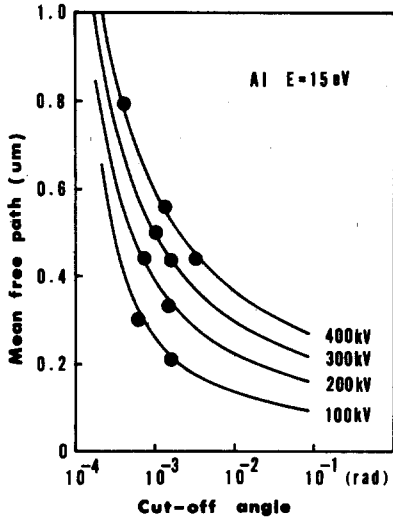


Fig. 5. Comparison between calculated and experimental mean-free-path lengths of the Al plasmon as a function of the cut-off angle and accelerating voltages. Experimental values are dark circles, whereas the calculated ones are solid lines.

plasmon energy,  $\epsilon$  is the relativistic correction factor and  $E_0$  the accelerating voltage.  $\lambda_p$  may also be obtained experimentally [7] by using

$$\lambda_p = \frac{t}{\ln(I_t/I_0)} \quad (3)$$

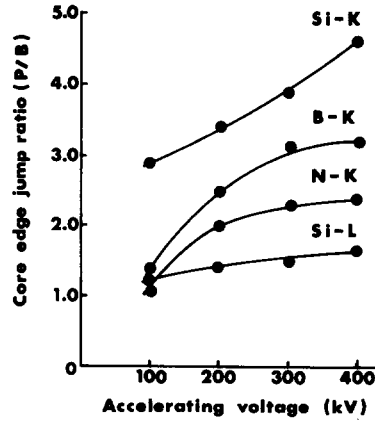


Fig. 7. Observed jump ratio for the  $Si_K$ ,  $Si_L$ ,  $B_K$  and  $N_K$  edges as a function of accelerating voltage.

Here  $t$  is the absolute specimen thickness,  $I_t$  the total intensity of the energy-loss spectrum, and  $I_0$  the intensity of the zero-loss peak. Then, the  $\lambda_p$  may be obtained from the EELS spectra shown in fig. 4. The continuum loss background peaks were subtracted from the total intensity [8] and the results are shown as dark circles. The experimental  $\lambda_p$  agree well with the theoretical values, which are shown as solid lines. As shown in fig. 5, the mean-free-path lengths vary with the cut-off angle as well as with the electron beam energy. The

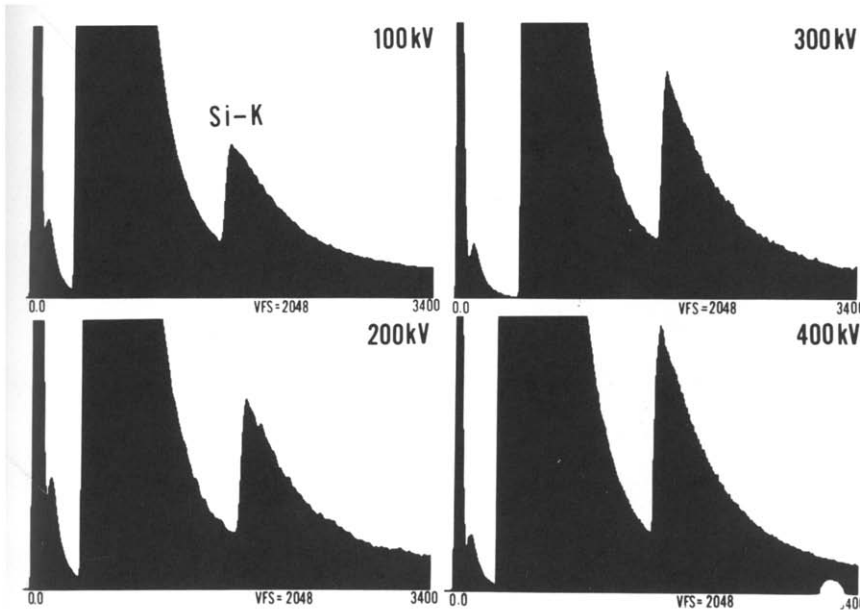


Fig. 6. EELS spectra from a 200 nm thick evaporated Si film, observed at voltages between 100 and 400 kV.  $Si_K$  edges are indicated.

mean-free-path lengths are 210, 320, 430 and 560 nm at 100, 200, 300 and 400 kV, respectively, with the cut-off angle of about 1.2 mrad.

Fig. 6 shows EELS spectra from a 200 nm thick evaporated Si film observed at different accelerating voltages. The cut-off angles are approximately 3.8 mrad. The characteristic loss peaks located at 1840 eV correspond to the  $\text{Si}_K$  edge. It is remarkable that the jump ratio of  $\text{Si}_K$  edge peak-to-background increases as the electron energy increases. The jump ratios are approximately 2.8, 3.5, 3.9 and 4.6 at 100, 200, 300 and 400 kV, respectively.

Fig. 7 shows the jump ratios observed for the  $\text{Si}_K$ ,  $\text{Si}_L$ ,  $\text{B}_K$  and  $\text{N}_K$  edges as a function of the accelerating voltages. The jump ratios increase continuously with the operating voltage. It is considered that the increase of the jump ratio at higher voltages is mainly due to the decrease of the background. Further details of the accelerating voltage dependence of the  $P/B$  ratio in both EDXS and EELS spectra will be published elsewhere, together with the same analysis of the reason for this, although many factors may be contributing.

### 2.3. Combined use of high-resolution imaging and microanalysis

Fig. 8 shows a high-resolution image of silicon aluminum oxynitride (sialon), for which the crystal

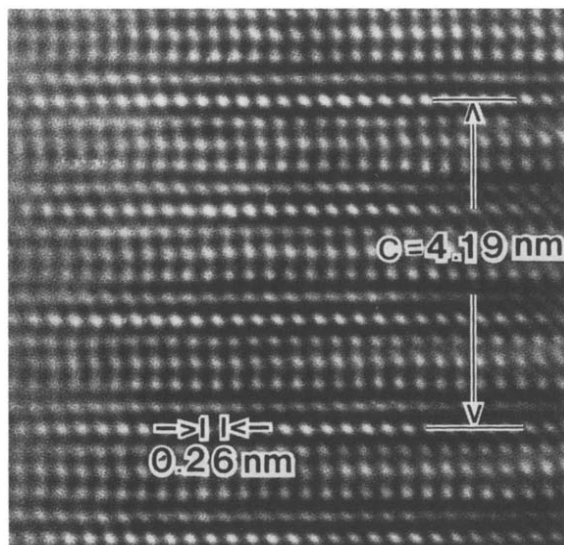


Fig. 8. A high-resolution image of a 15R silicon aluminum oxynitride polytype. Cation sites are well resolved as dark dots. The separation between the dark dots normal to the  $c$  axis is 0.26 nm.

structure and chemical composition was not well understood. The direct magnification was  $3 \times 10^5$  times and the exposure time 2 s. The image was obtained at the optimum defocus of about 90 nm. Selected area electron diffraction patterns and convergent-beam electron diffraction patterns suggested that the crystal had hexagonal symmetry,

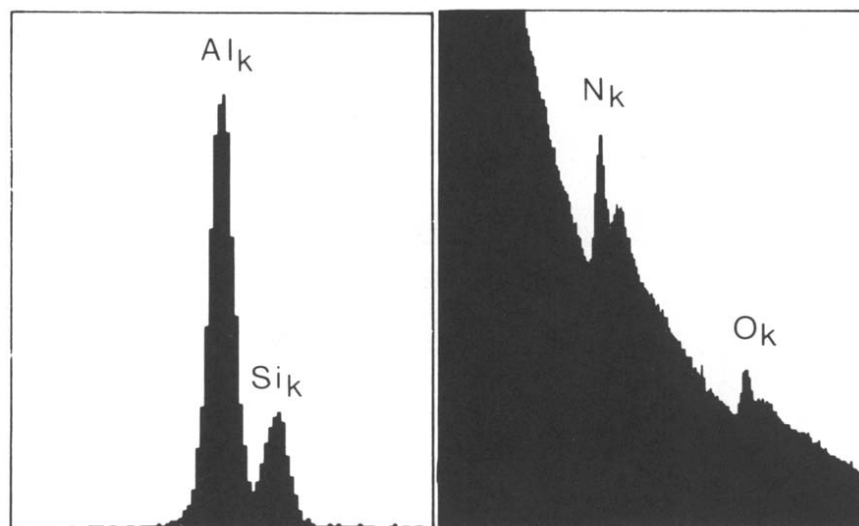


Fig. 9. Corresponding EDXS (a) and EELS (b) spectra, obtained successively from the same crystal fragment as observed in fig. 8. The chemical composition was determined to be  $\text{SiAl}_4\text{O}_2\text{N}_4$ .

with lattice parameters  $a = 0.301$  and  $c = 4.19$  nm. From the length of the  $c$  axis, it was deduced that the present crystal belongs to a 15R polytype [9]. The cation sites appear well resolved in the image as dark dots, whereas white dots correspond to vacant tetrahedral and octahedral sites. The distance between the dark dots is 0.26 nm normal to the  $c$  axis.

Figs. 9a and 9b show EDXS and EELS spectra, obtained successively from the same crystal fragment as observed in fig. 8. The characteristic X-ray peaks are assigned to  $Al_K$  and  $Si_K$  lines in fig. 9a. Fig. 9b shows the  $N_K$  and  $O_K$  edges at 402 and 532 eV, respectively. On the basis of the thin film approximation for the EDXS spectra and use of experimental  $k$  factors, the molar ratio of Si to Al was estimated to be 1:4. The experimental error was within 2%. On the other hand, quantitative analysis of the EELS spectra, carried out using the Egerton program, gave the molar ratio of O to N as 2:4. The error was about 20%. Combining the results of the EDXS and EELS analysis, the chemical composition of the 15R sialon polytype was  $SiAl_4O_2N_4$ .

Combination of both the structure images and the spectroscopic analysis leads to a structure model, which may be described as an alternate packing of tetrahedral and octahedral polyhedra in layers perpendicular to the  $c$  axis. The result of the structure analysis will be published elsewhere.

### Acknowledgements

The authors would like to express their deep gratitude to Dr. M. Mitomo for supplying crystals

and Mr. Y. Kitami for help with the experiment. They also thank Dr. L.A. Bursill, University of Melbourne, for reading the manuscript. The present work has been supported by the special coordination fund for promotion of Science and Technology from the Science and Technology Agency of the Japanese Government.

### References

- [1] N.J. Zaluzec, A. Taylor, E.A. Ryan and A. Philippides, in: Proc. 7th Intern. Conf. on High Voltage Electron Microscopy, Berkeley, CA, 1983, p. 81.
- [2] G. Zanchi, Y. Kihn, J. Sevely and B. Jouffrey, in: Proc. 7th Intern. Conf. on High Voltage Electron Microscopy, Berkeley, CA, 1983, p. 85.
- [3] H. Hashimoto, H. Endoh, T. Honda, Y. Harada, S. Sakurai and T. Etoh, in: Proc. 7th Intern. Conf. on High Voltage Electron Microscopy, Berkeley, CA, 1983, p. 15.
- [4] Y. Bando, Y. Matsui, Y. Kitami, Y. Inomata, K. Ibe, T. Honda and Y. Harada, Japan. J. Appl. Phys. 23 (1984) L414.
- [5] Y. Bando, Y. Matsui, Y. Kitami and Y. Inomata, JEOL News 22 (1984) 28.
- [6] C. Colliex, Electron Energy Loss Spectroscopy in the Electron Microscope, in: Advances in Optical and Electron Microscopy (North-Holland, Amsterdam, in press).
- [7] N.J. Zaluzec, in: Proc. 38th Annual EMSA Meeting, San Francisco, CA, 1980, Ed. G.W. Bailey (Claitor's, Baton Rouge, LA, 1980) p. 112.
- [8] L. Marton, J.A. Simpson, H.A. Fowler and N. Swanson, Phys. Rev. 126 (1962) 182.
- [9] K.H. Jack, J. Mater. Sci. 11 (1976) 1135.